AD-A134 318 ACCELERATION AND CONFINEMENT OF ENERGETIC PARTICLES IN THE 7 JUNE 1980 SO..(U) ARROSPACE CORP EL SEGUNDO CA SPACE SCIENCES LAB S R KANE ET AL. 31 AUG 83 1/1

UNCLASSIFIED TR-0083(3940-01)-2 SD-TR-83-66 F/G 3/2 NL

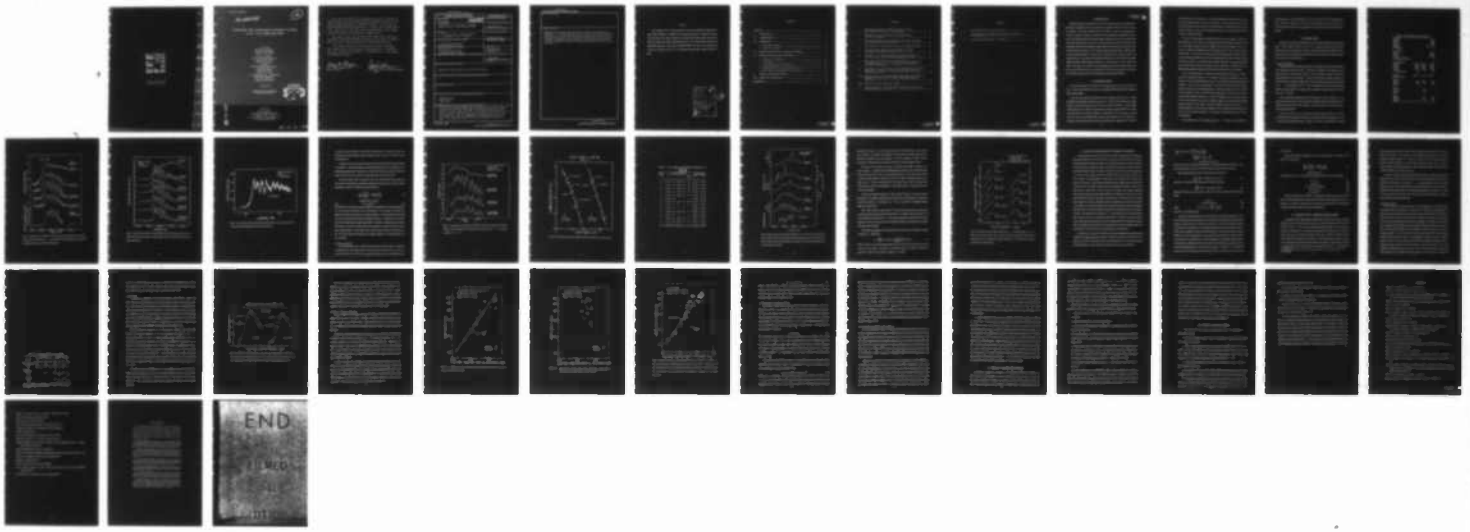

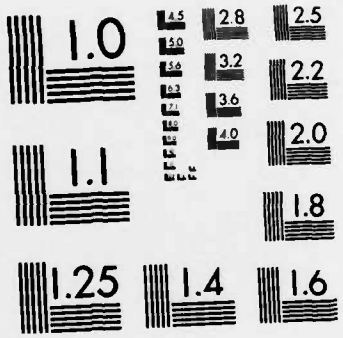

REPORT NO SD-TR-83-66

(12)

Acceleration and Confinement of Energetic Particles in the 7 June 1980 Solar Flare

S. R. KANE
Space Sciences Laboratory
University of California
Berkeley, Calif. 94720

K. KAI, T. KOSUGI
Tokyo Astronomical Observatory
University of Tokyo
Mitaka, Tokyo, Japan

S. ENOME
Research Institute of Atmospherics
Nagoya University
13 Honohara 3-Chome
Toyokawa 442, Japan

P. B. LANDECKER, D. L. McKENZIE
Space Sciences Laboratory
Laboratory Operations
El Segundo, Calif. 90245

31 August 1983

Prepared for

SPACE DIVISION
AIR FORCE SYSTEMS COMMAND
Los Angeles Air Force Station
P.O. Box 92960, Worldway Postal Center
Los Angeles, Calif. 90009

This report was submitted by The Aerospace Corporation, El Segundo, CA 90245, under Contract No. F04701-82-C-0083 with the Space Division, P.O. Box 92960, Worldway Postal Center, Los Angeles, CA 90009. It was reviewed and approved for The Aerospace Corporation by H. R. Rugge, Space Sciences Laboratory. Captain Gary M. Rowe, SD/YC, was the project officer for the Mission Oriented Investigation and Experimentation (MOIE) Program.

This report has been reviewed by the Public Affairs Office (PAS) and is releasable to the National Technical Information Service (NTIS). At NTIS, it will be available to the general public, including foreign nationals.

This technical report has been reviewed and is approved for publication. Publication of this report does not constitute Air Force approval of the report's findings or conclusions. It is published only for the exchange and stimulation of ideas.

Gary M. Rowe

Gary M. Rowe, Captain, USAF
Project Officer

Joseph Hess

Joseph Hess, GM-15, Director
West Coast Office, AF Space Technology Center

UNCLASSIFIED

SECURITY CLASSIFICATION OF THIS PAGE (When Data Entered)

REPORT DOCUMENTATION PAGE		READ INSTRUCTIONS BEFORE COMPLETING FORM
1. REPORT NUMBER SD-TR-83-66	2. GOVT ACCESSION NO. A134318	3. RECIPIENT'S CATALOG NUMBER
4. TITLE (and Subtitle) Acceleration and Confinement of Energetic Particles in the 7 June 1980 Solar Flare		5. TYPE OF REPORT & PERIOD COVERED TR-0083(3940-01)-2 6. PERFORMING ORG. REPORT NUMBER
7. AUTHOR(s) S. R. Kane, K. Kai, T. Kosugi, S. Enome, P. B. Landecker, and D. L. McKenzie		8. CONTRACT OR GRANT NUMBER(s) F04701-82-C-0083
9. PERFORMING ORGANIZATION NAME AND ADDRESS The Aerospace Corporation El Segundo, Calif. 90245		10. PROGRAM ELEMENT, PROJECT, TASK AREA & WORK UNIT NUMBERS
11. CONTROLLING OFFICE NAME AND ADDRESS Space Division Air Force Systems Command Los Angeles, Calif. 90009		12. REPORT DATE 31 August 1983 13. NUMBER OF PAGES 42
14. MONITORING AGENCY NAME & ADDRESS(if different from Controlling Office)		15. SECURITY CLASS. (of this report) Unclassified 15a. DECLASSIFICATION/DOWNGRADING SCHEDULE

16. DISTRIBUTION STATEMENT (of this Report)

Approved for public release; distribution unlimited.

17. DISTRIBUTION STATEMENT (of the abstract entered in Block 20, if different from Report)

18. SUPPLEMENTARY NOTES

19. KEY WORDS (Continue on reverse side if necessary and identify by block number)

microwave bursts
solar flares
X-ray bursts

20. ABSTRACT (Continue on reverse side if necessary and identify by block number)

Pulsations with large amplitude and duration have been observed during the hard X-ray and microwave radio bursts associated with the 7 June 1980 (~ 0312 UT) solar flare. The high time resolution measurements of 20-800 keV X-rays were made with the X-ray spectrometers aboard the ISEE-3 and P78-1 spacecraft. The radio measurements, covering metric to microwave wavelengths, were made at the Nobeyama and Toyokawa observatories in Japan. The temporal evolution of the X-ray and radio spectra and the

DD FORM (FACSIMILE) 1473

UNCLASSIFIED

SECURITY CLASSIFICATION OF THIS PAGE (When Data Entered)

19. KEY WORDS (Continued)

20. ABSTRACT (Continued)

polarization and spatial structure of the microwave source have been examined. The following interpretation is found to be consistent with the observations: (1) the variations in the electron acceleration/injection spectrum are responsible for the observed variations in the hard X-ray and microwave emissions; (2) the locations of the hard X-ray and microwave sources are probably different, the X-ray source being located at a lower altitude.

PREFACE

We are grateful to Dr. A. Gordon Emslie for his careful reading of the manuscript and many helpful comments. At Berkeley, the processing and analysis of the ISEE-3 X-ray data were supported by the National Aeronautics and Space Administration under contract NAS5-25980; the analysis was partially supported also by the U. S. Air Force Systems Command (AF Geophysics Laboratory) under contract F19628-80-C-0208. The work at the Aerospace Corporation was supported by the U. S. Air Force Space Division under contract F04701-81-C-0082.

CONTENTS

FIGURES

TABLES

I. INTRODUCTION

Rapid fluctuations in the hard X-ray and microwave radio emissions from solar flares have been under investigation for about a decade [*Parks and Winckler*, 1969; *Frost*, 1969; *Anderson and Mahoney*, 1974; *Hurley and Duprat*, 1977; *Lipa*, 1978]. A study of such fluctuations is expected to provide an insight into the process of particle acceleration, especially that of electrons. The fluctuations observed in the past typically consisted of a few (3 to 4) quasi-periodic pulses with periods between 10 and 100 sec. Recently some of us reported a flare with rather well-defined quasi-periodic oscillations of large amplitude in hard X-ray and microwave radio emissions observed, respectively, with the International Sun Earth Explorer-3 (ISEE-3) spacecraft and the ground-based radio observatories in Japan [*Kane, Kai, and Enome*, 1980]. The flare occurred on 7 June 1980 and was also observed with the U.S. Air Force P78-1 and Solar Maximum Mission (SMM) satellites [*Kiplinger et al.*, 1980; *Chupp et al.*, 1981; *Forrest et al.*, 1981]. In this paper, we present the so-far unpublished X-ray and radio observations of this flare in some detail and discuss their implications in terms of the characteristics of the impulsive X-ray and microwave sources and the acceleration of particles in solar flares.

II. INSTRUMENTATION

The X-ray observations were made with instruments aboard two spacecraft, ISEE-3 and P78-1. The radio observations were made at ground-based observatories located at Nobeyama and Toyokawa in Japan.

The X-ray spectrometer aboard ISEE-3 has been described earlier [*Kane et al.*, 1982]. The ISEE-3 data discussed in this paper consist of 26 - 3170 keV X-rays covered in 12 energy channels. The basic time resolution is 0.5 sec for 26 - 398 keV X-rays and 1 - 4 sec for higher energy channels. The Aerospace Corporation X-ray experiment aboard USAF P78-1 satellite has been described by *Landecker, McKenzie and Rugge* [1979]. The measurements discussed here were made with the MONEX High Energy Monitor (HEM) part of the instrument. It consists of a xenon-filled proportional counter which measures the integral flux of 20 - 250 keV

X-rays with 0.032 sec. time resolution. A six channel differential X-ray spectrum is also measured in this energy range with 1.024 sec time resolution. The X-ray spectra measured with the P78-1 instrument have been compared with those measured by the ISEE-3 instrument during several solar flares. The two sets of measurements are found to be in good agreement [*Kane, Landecker, and McKenzie*, 1982].

The two X-ray spectrometers complement each other in several respects. Although the HEM instrument covers a smaller X-ray energy range than does the ISEE-3 instrument, in the 20 - 93 keV range, the spectral resolution of HEM is better than that of ISEE-3 by about a factor of two. Moreover, the HEM covers the X-ray energy range 20 - 26 keV, which is not measured by ISEE-3. Also, unlike the lower energy channel measurements from the ISEE-3 instrument, the HEM measurements do not have spin modulation effects, since the HEM is pointed continuously at the Sun. On the other hand, the ISEE-3 instrument has a large dynamic range and can measure X-ray spectra from medium as well as large flares. The HEM, however, is affected by gain changes in large flares where the total counting rate is $\gtrsim 10^4$ counts/sec.

The 17 GHz interferometer at Nobeyama has been described by *Nakajima et al.* [1980]. It consists of 14 paraboloidal reflectors of 1.2 m diameter. The antenna arrangement is of a compound type. The fundamental spacing d_0 is 96.4 λ (λ: wavelength) and the maximum spacing is 3856 λ (= 40 d_0) in the east-west direction. Forty Fourier components of the Sun's brightness are recorded with a multi-correlator system. If the direct inversion of the forty observed Fourier components is made, the FWHM of the observing beam is 49" and 33" with the Hanning and flat data windows, respectively. In case of a compact source, a more precise estimate of the size and position of the source is possible through the new model fitting technique recently developed by *Kosugi* [1982]. When this technique is used, the uncertainty is < 5". East-west profiles of the whole Sun are produced for LH- and RH-circular polarizations once every 0.8 s at the maximum sampling rate. The minimum detectable flux density is 0.6 sfu for 0.8 s integration.

Five polarimeters cover the frequency range of 1 - 17 GHz. Four polarimeters at

Toyokawa [*Torri et al.*, 1979] are operated at 1.0, 2.0, 3.75 and 9.4 GHz; the remaining polarimeter at Nobeyama is operated at 17 GHz. For all the polarimeters, the time constants are 0.3 sec and the measurements of circular polarization are essentially simultaneous at all the five frequencies.

III. OBSERVATIONS

The general observational characteristics of the 7 June 1980 solar flare are summarized in Table 1. The Hα flare was located at $N12°$, $W74°$. Although the optical flare was only of importance SN, the radio emission in the metric, decimetric, and microwave regions was quite intense. The flare was associated with impulsive hard X-ray and microwave bursts and type II, III, IV, and V radio bursts of intensity 3.

(a) Hard X-Ray Emission

The time-counting rate profiles of the hard X-ray emission observed with the ISEE-3 and P78-1 instruments are shown in Figure 1 and Figure 2, respectively. For comparison, the 17 GHz radio emission is also shown in Figure 1. The X-ray emission consists of a rapid initial increase followed by a series of pulses. A total of seven peaks can be clearly identified. The P78-1 data shows an additional eighth peak. The time between the successive seven peaks P_1, P_2, $\cdots$ P_7 is approximately 5.5, 9, 8, 12.5, 7 and 8 seconds, respectively, the average time between the peaks being about 8 seconds. The time between P_7 and the peak P_8 in the P78-1 data is also $\sim$ 8 seconds.

It is of considerable interest to know if a sub-structure on a finer time scale ($<$ 1 sec) existed in this event. Figure 3 shows the high time resolution (0.032 sec) measurements of X-rays $\gtrsim$20 keV made with the P78-1 instrument. There is no indication of a sub-structure on a $\gtrsim$32 millisecond time scale.

The X-ray peaks tend to be more pronounced at high energies ($\gtrsim$100 keV). For example, the ratio of the counting rate at the peak P_4 to that at the valley V_4 increases from $\sim$1.1 to $\sim$6 as the X-ray energy increases from $\sim$20 keV to $\sim$100 keV. In fact, the peaks P_5 through

Table 1. Characteristics of 7 June 1980 Flare

Hα emission			
Start (UT)			<0319
Max (UT)			~0319
End (UT)			≥0322
Importance			SN
Location			N12°, W74°
McMath Region			
X-rays ≥20 keV			
Start (UT)			0311.8
Max (UT)			~0312.25
End (UT)			~0313.5
Peak Flux at ~30 keV (photons cm^{-2} sec^{-1} keV^{-1})			~32
Microwave Emission			
Frequency	3.7 GHz	9.4 GHz	17 GHz
Start (UT)	~0312.1	~0312.1	~0312.1
Max (UT)	~0312.8	~0312.7	~0312.5
End (UT)	~0314	~0314	~0313.1
Peak Flux (10^{-22} WM^{-2} Hz^{-1})	132	500	1000
Metric and Decimetric Emission	*decimetric*	*metric*	*dekametric*
Type III, V			
Start (UT)	0312	0311.5	0312
End (UT)	0314	0314	0314
Intensity	3	3	3
Type II			
Start (UT)	–	0313	–
End (UT)	–	0332	–
Intensity	–	3	–
Type IV			
Start (UT)	–	0314	0314
End (UT)	–	0325	0318
Intensity	–	3	3

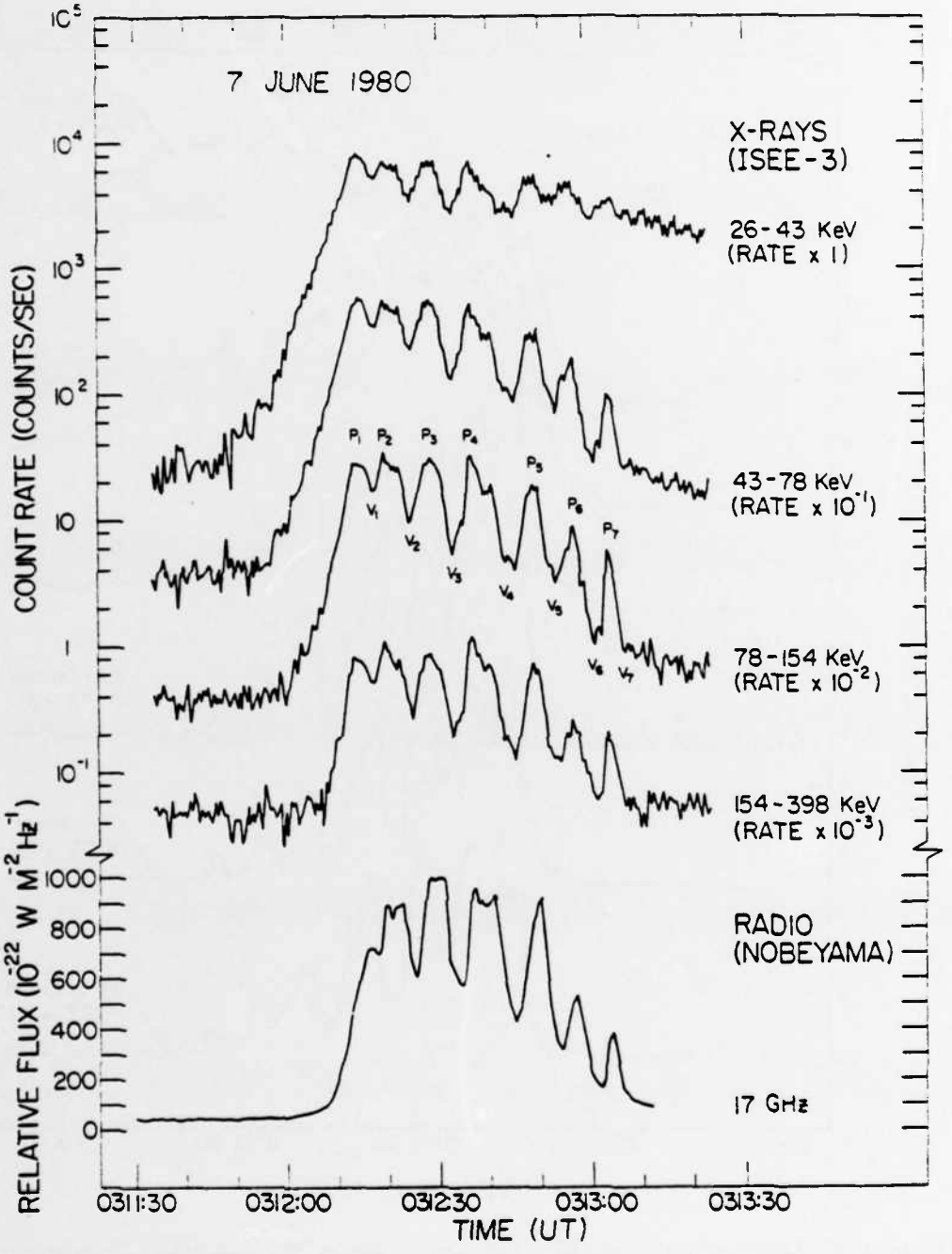

Figure 1. Time-intensity plot of 26-398 keV X-ray and 17 GHz radio emission during the 7 June 1980 flare. Note the seven distinctive peaks (P_1, P_2, $\cdots$ P_7) in both the X-ray and radio emissions. The intensity scale is logarithmic for the X-ray and linear for the radio emission.

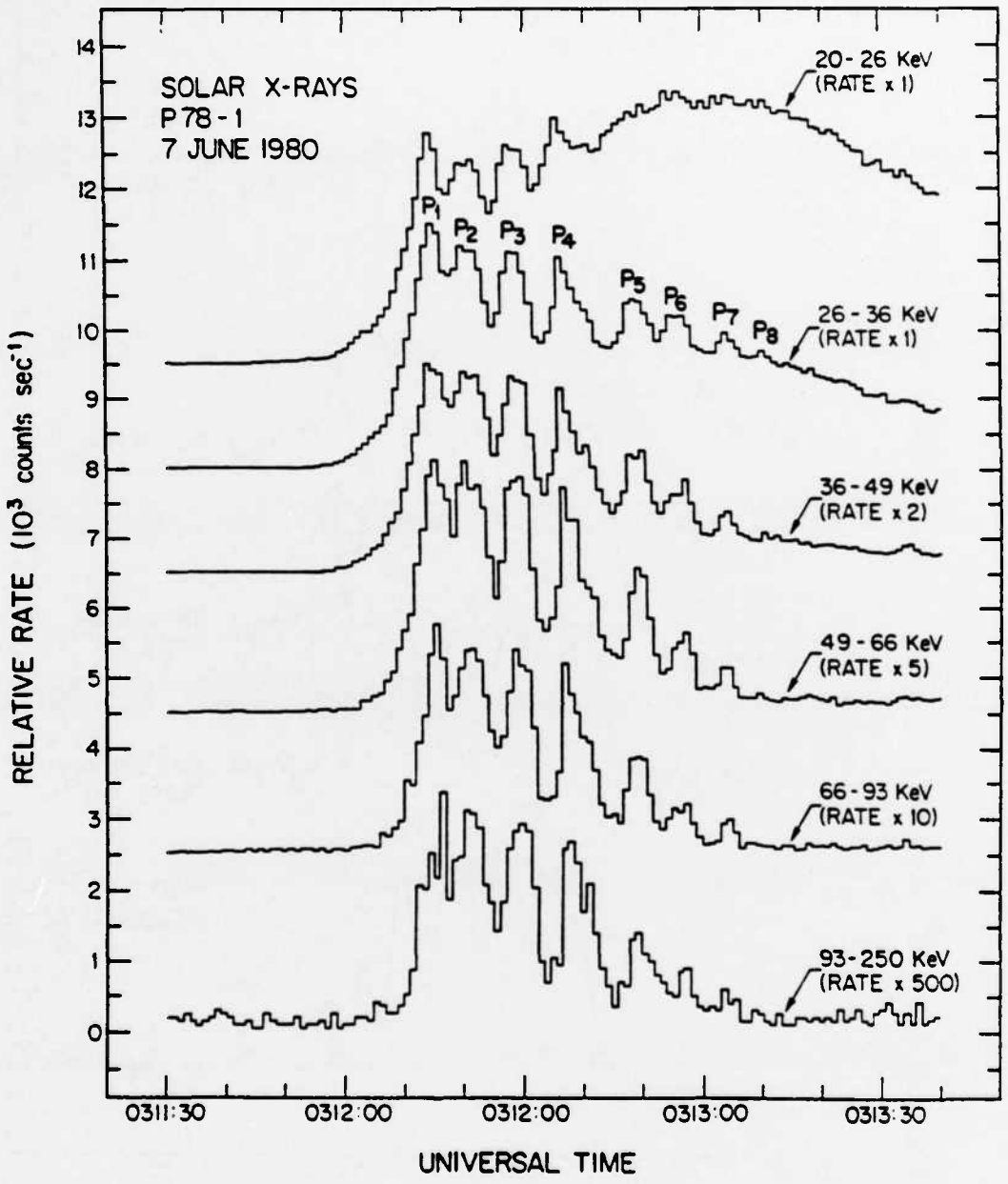

Figure 2. Time-rate plot for 20-250 keV X-rays observed with the P78-1 instrument. Both time and rate scales are linear. Note the seven peaks P_1 through P_7 similar to those observed by ISEE-3 (Figure 1) and a possible eighth peak P_8.

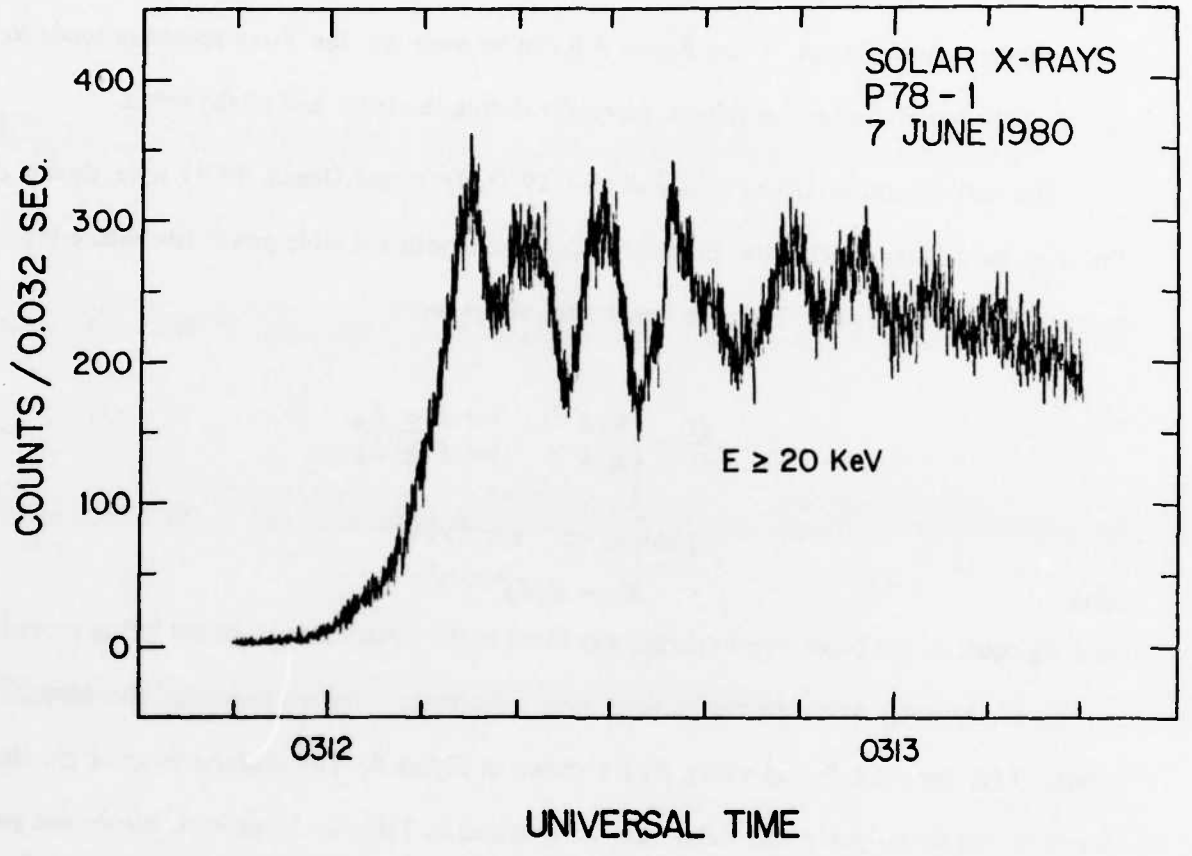

Figure 3. The counting rate of X-rays observed by the P78-1 instrument with a time resolution of 0.032 sec. Note the absence of any significant time structure with small time scales.

P_7 cannot be clearly identified in the 20-26 keV range (Figure 2). Instead, the 20-26 keV counting rate increases gradually, reaches a maximum value at the time of the peak P_6, and then decays slowly.

In Figure 4, we present the time variation of the ratios of several X-ray channels between 20 and 400 keV. An increase in each ratio indicates the hardening of the X-ray spectrum in the corresponding energy range. From Figure 4 it can be seen that the X-ray spectrum tends to be harder at the peaks than at the valleys, especially during the latter half of the event.

The earlier studies [*Kane and Anderson*, 1970; *Frost and Dennis*, 1971] have shown that the solar hard X-ray spectra are, in general, consistent with a double power law with a break at an energy of $\sim$ 100 keV. Therefore a spectrum of the form

$$\frac{dj}{dE} = \begin{cases} K_1 E^{-\gamma_1} & \text{for } E \leq E_B \\ K_2 E^{-\gamma_2} & \text{for } E \geq E_B \end{cases} \qquad (1)$$

$$\text{photons cm}^{-2}\,\text{sec}^{-1}\,\text{keV}^{-1}$$

with
$$K_2 = K_1 E_B^{(\gamma_2 - \gamma_1)} \qquad (2)$$

and E_B equal to the break-point energy, was fitted to the observations. In the fitting procedure, γ_1, γ_2, K_1 and E_B were treated as four free parameters. As an example, the spectral fits obtained for the peak P_1 and valley V_4 are shown in Figure 5. The characteristics of the similar fits to all the seven peaks and valleys are summarized in Table 2. In general, the double power law fits are consistent with the present observations. The spectra at the peaks tend to be harder than those at the valleys, the effect being more pronounced for X-rays $\lesssim$ 100 keV than for those of higher energy. It is also possible to fit 'thermal' spectra to some of the peaks and valleys. The results obtained in this paper do not depend critically on the assumed shape of the X-ray spectrum.

(b) Microwave Emission

The observed profile of the 17 GHz flux has already been shown in Figure 1. In Figure 6 we present the time-flux profiles observed at several frequencies between 1 and 17 GHz. Like the hard X-ray flux, the 17 GHz flux also undergoes fluctuations with seven identifiable peaks,

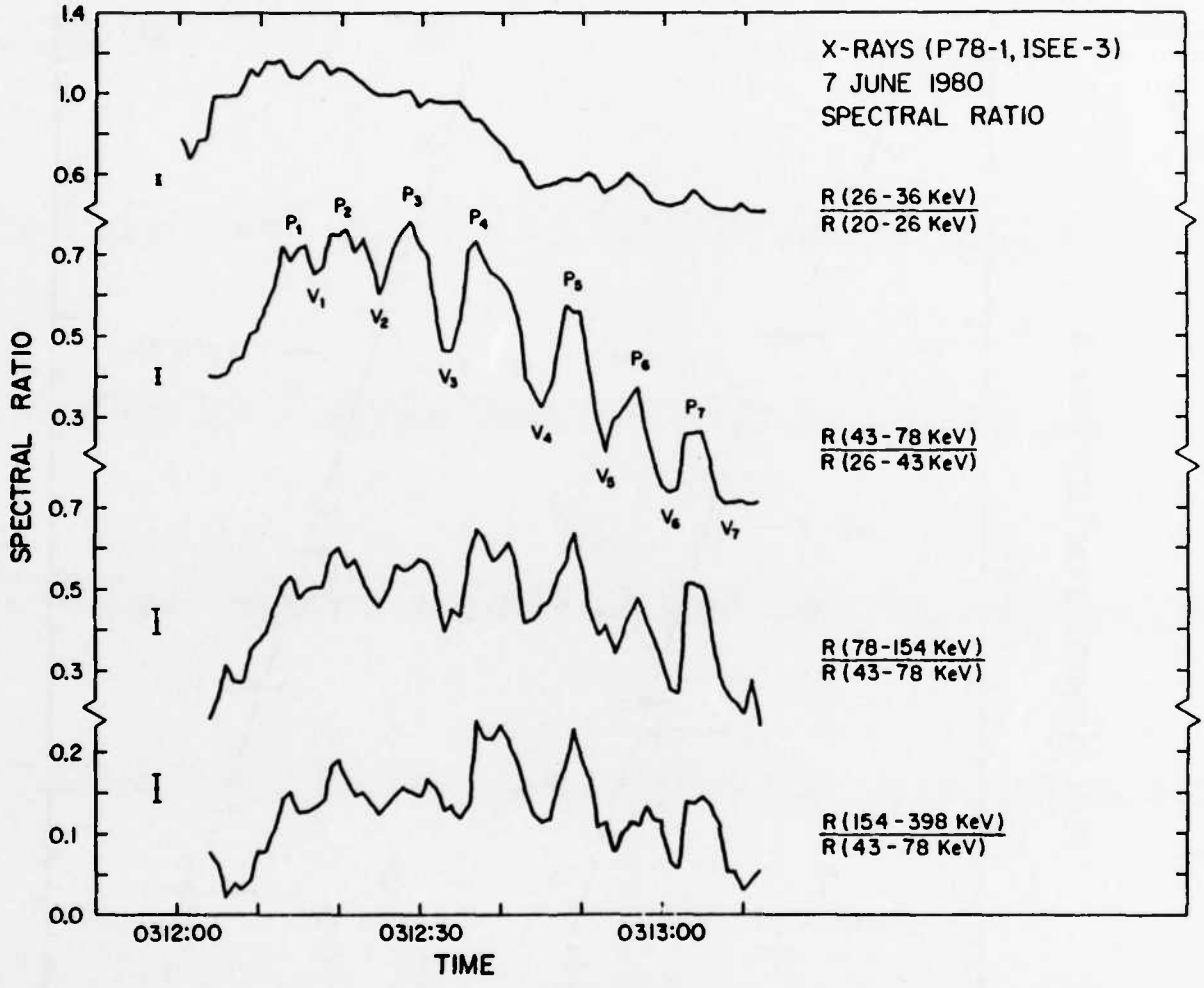

Figure 4. Time variation of the spectral ratios for 20-398 keV X-rays. The error bars show the statistical uncertainty. Note the hardening of the spectrum (large ratio) near the peaks P_1, P_2, $\cdots$ P_7 as compared to the valleys V_1, V_2, $\cdots$ V_7.

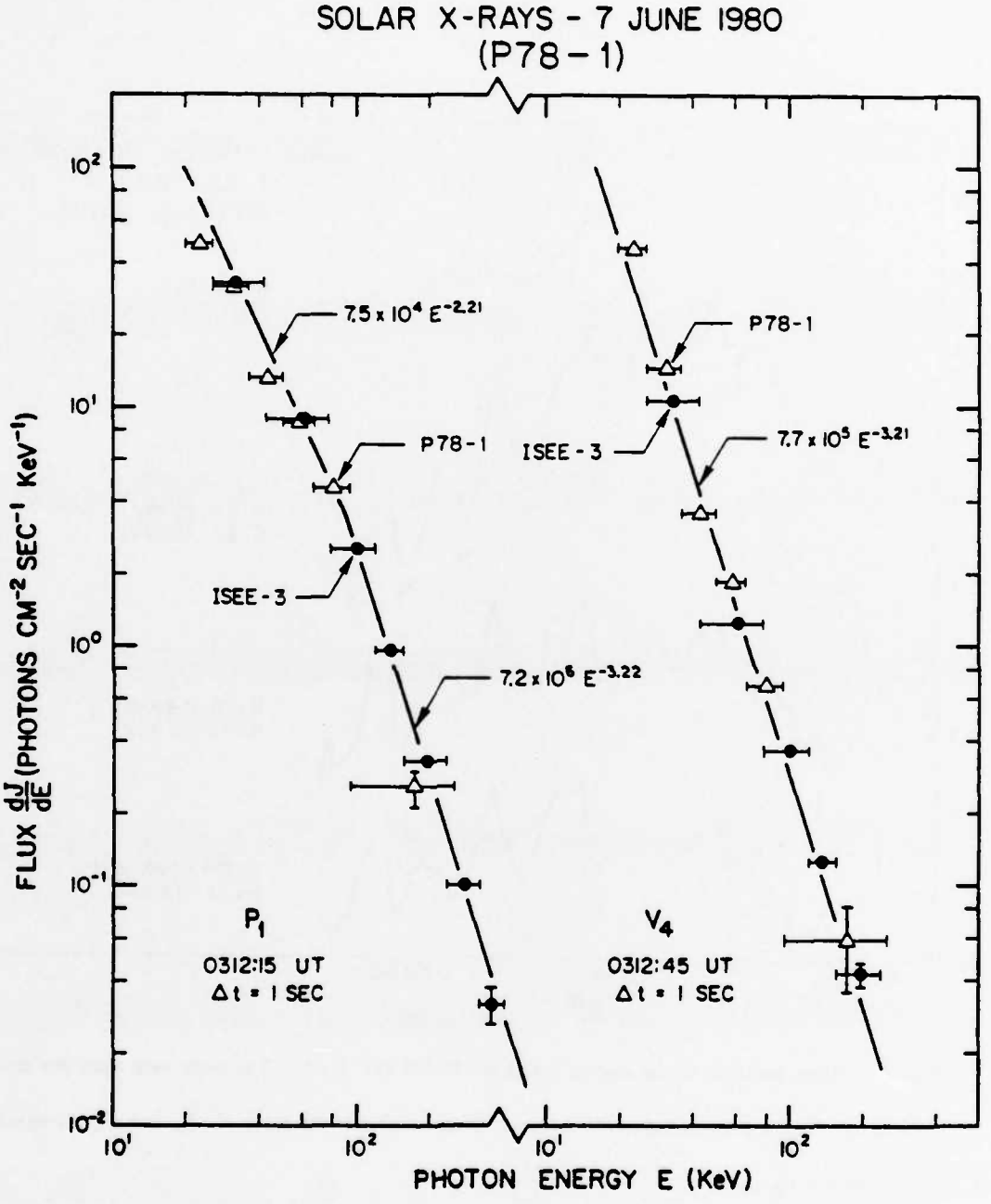

Figure 5. The X-ray spectra observed with the ISEE-3 and P78-1 instruments at the peak P_1 and valley V_4.

Table 2. X-ray Spectra and Deduced Characteristics of Electrons (7 June 1980)

Peak or Valley	X-ray Spectral Parameters					N_e (electrons/sec)	
	K_1	γ_1	K_2	γ_2	E_B (keV)	$\geq$25 keV	$\geq$100 keV
P_1	7.5×10^4	2.2	7.2×10^6	3.2	93	6.7×10^{35}	2.4×10^{34}
V_1	6.1×10^4	2.3	1.9×10^6	3.0	95	3.6×10^{35}	1.3×10^{34}
P_2	8.0×10^3	1.6	1.3×10^6	2.8	69	3.4×10^{35}	1.9×10^{34}
V_2	5.3×10^4	2.4	5.2×10^5	2.9	67	2.1×10^{35}	6.1×10^{33}
P_3	5.2×10^3	1.5	3.8×10^6	3.1	69	4.0×10^{35}	2.1×10^{34}
V_3	2.5×10^5	2.9	–	–	–	1.7×10^{35}	3.3×10^{33}
P_4	5.9×10^4	2.2	6.4×10^6	3.1	189	5.4×10^{35}	2.5×10^{34}
V_4	7.7×10^5	3.2	–	–	–	2.3×10^{35}	2.7×10^{33}
P_5	1.3×10^5	2.5	–	–	–	2.0×10^{35}	6.3×10^{33}
V_5	1.2×10^{10}	6.0	1.6×10^5	2.9	37	6.6×10^{35}	1.9×10^{33}
P_6	1.3×10^6	3.2	–	–	–	3.9×10^{35}	4.6×10^{33}
V_6	9.9×10^9	6.0	1.0×10^5	3.1	51	4.5×10^{35}	5.5×10^{32}
P_7	1.1×10^{10}	6.0	8.4×10^4	2.7	36	5.7×10^{35}	2.1×10^{33}
V_7	9.9×10^9	6.0	9.3×10^3	2.7	65	2.6×10^{35}	2.4×10^{32}

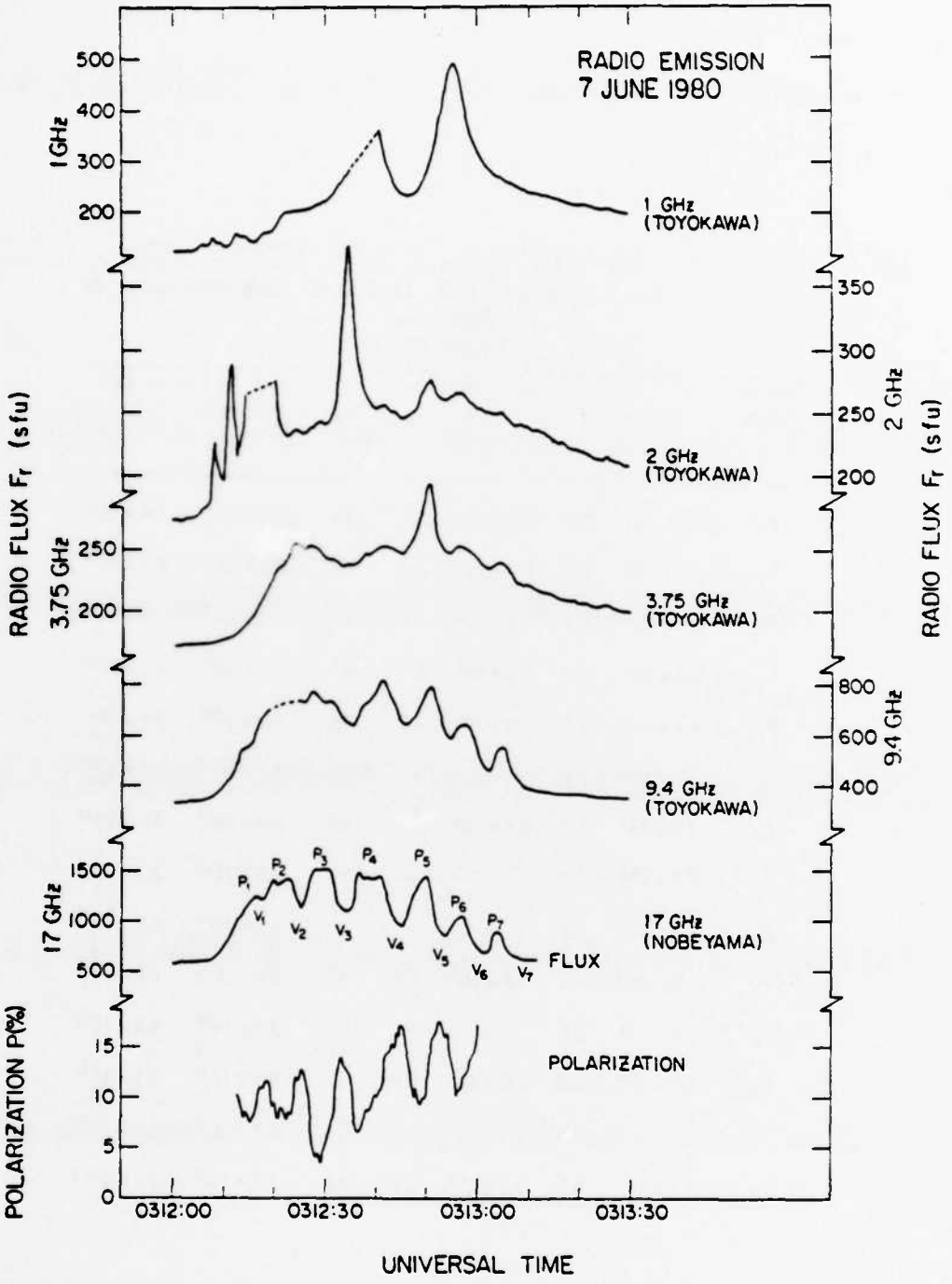

Figure 6. Comparison of the time variations of the radio fluxes at 1, 2, 3.75, 9.4, and 17 GHz and the polarization at 17 GHz. The radio flux shown includes the quiet sun component. Note (1) the overall variation is much more similar to the X-ray emission (Figure 1) for frequencies > 3.75 GHz; (2) the polarization is large at the valleys and small at the peaks.

although the first peak, P_1, is not as clearly evident in the 17 GHz data as it is in the X-ray data. Moreover, the regularity and magnitude of the fluctuations decreases rapidly with the decrease in the frequency of the radio emission. In fact, at frequencies $\lesssim$ 3 GHz, the flux is dominated by variations which do not seem to be related to the seven peaks and valleys.

The microwave radio spectra at the peaks P_2 through P_7 and valleys V_3 through V_6 are shown in Figure 7. The spectra at the remaining peaks and valleys were not constructed either because of incomplete data or due to a very small radiation flux. It can be seen that the spectra at the early peaks continue to rise from 3.75 GHz to 17 GHz, the maximum being at a frequency $f_{max} > 17$ GHz. On the other hand, at the valleys $f_{max} \lesssim 17$ GHz. Thus the spectra at the peaks and valleys are quite different. In both cases, however, f_{max} decreases with time as the event progresses.

The circular polarization observed at 17 GHz is shown in Figure 6. The burst is partially RH polarized. The degree of polarization p varies with time, p increasing with the decrease in the total flux density F. At the peaks p is 5 - 10%. At the valleys p is significantly larger, being in the range 10-20%.

The 17 GHz radio source was located at 15' 10" west of the solar disk center, the center of the position being constant during the event within $\sim$ 3" during the entire radio burst. The size of the source is estimated to be $<$ 5" with no detectable change during the burst. Thus the position and size of the radio source were essentially constant even though the flux density underwent large fluctuations.

The brightness temperature T_b of the radio source is related to the flux density F through the relation (cf. *Kundu*, 1965)

$$F = \frac{2kT_b}{\lambda^2}\Omega = 1.88\times10^{-27}\left[\frac{\Omega}{\Omega_\odot}\right]\frac{T_b}{\lambda^2}\ Wm^{-2}\,Hz^{-1} \qquad (3)$$

where Ω and $\Omega_\odot$ are the solid angles subtended by the burst source and sun's disk, respectively, and λ is in meters. For instance, the measured value of $F = 1000$ sfu at the peak P_3 gives $T_b = 3\times10^9$ K. For the valley V_3, we get $T_b = 1.5\times10^9$ K.

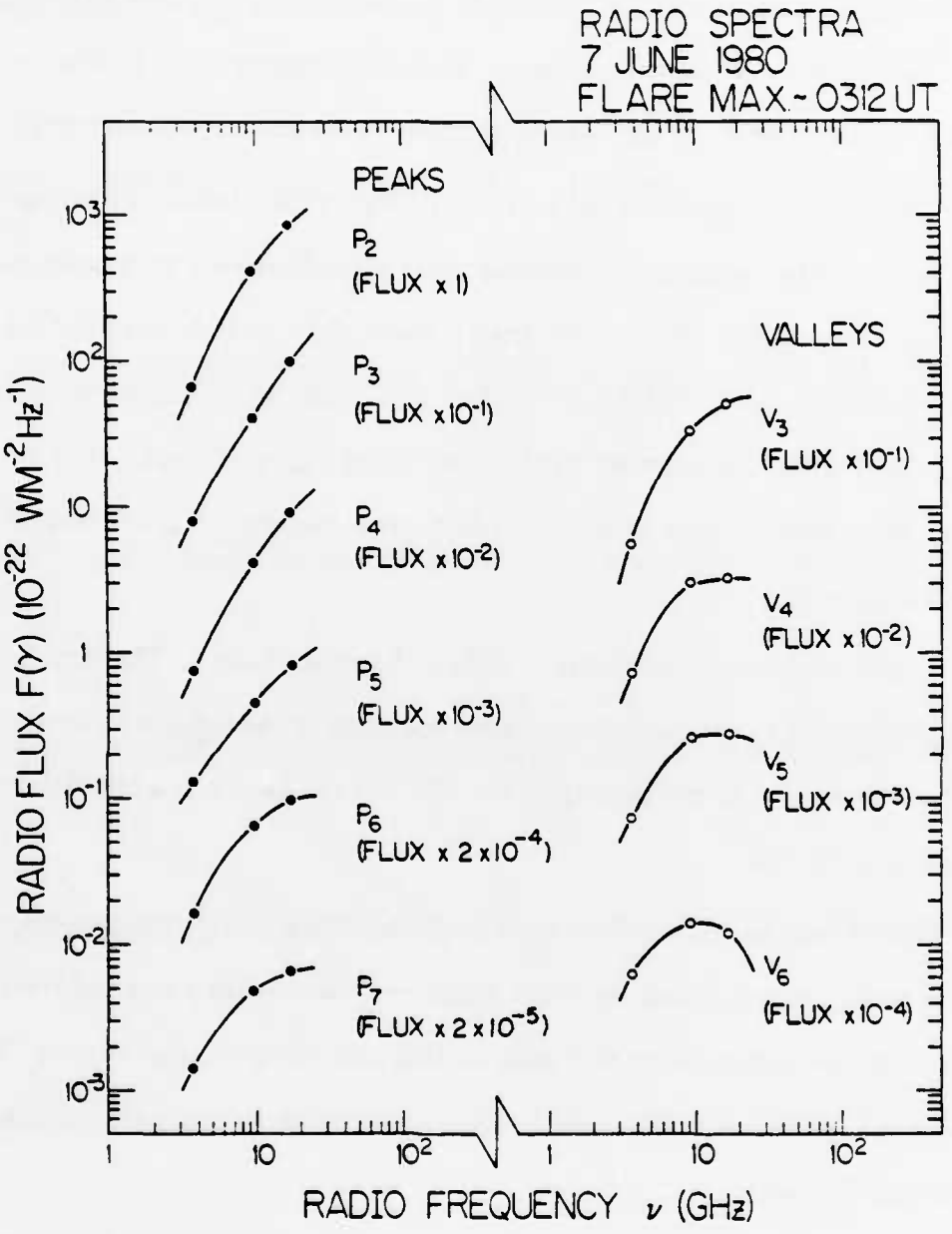

Figure 7. Radio spectra at the time of intensity peaks P_2, P_3, $\cdots$ P_7 and intensity valleys V_3, V_4, V_5, V_6 (valley V_i lies between the peaks P_i and P_{i+1}). Note that, in general, the steepness of the radio spectrum decreases with time. Also the frequency of maximum emission f_{max} is > 17 GHz for the intensity peaks and $\lesssim 17$ GHz for the intensity valleys.

IV. DEDUCED CHARACTERISTICS OF ENERGETIC ELECTRONS

If the characteristics of the hard X-ray source are known, information about the energetic electrons responsible for the X-ray emission can be obtained from the observed X-ray spectra. The measurements of the spatial structure of $\gtrsim$ 100 keV X-ray sources in flares have shown that the X-ray source is located relatively low in the solar atmosphere at an altitude $\lesssim$ 2500 km above the photosphere [*Kane et al.*, 1982]. Observations of the sources of lower energy X-rays ($\sim$ 20 keV) are also consistent with the low altitude of the hard X-ray source [*Hoyng et al.*, 1981]. Because of the high density of ambient gas in a low altitude source, the hard X-ray emission is expected to be thick-target bremsstrahlung from energetic electrons injected into the X-ray source. The energetic electrons could be accelerated either locally, inside the X-ray source itself, or more likely, in the low corona, from whence they propagate downwards towards the photosphere along the magnetic field lines. Depending on the details of the magnetic field structure and other propagation characteristics of the electrons, the X-ray emission will be anisotropic and hence corrections may have to be made to the observed X-ray spectrum for the effects of the observation angle and the backscatter of photons from the photosphere. At present there is no direct information available about the anisotropy of the X-ray emission at the source. The observations at a distance of $\sim$ 1 A.U. from the flare do not show any dependence of the X-ray flux on the observation angle [*Kane et al.*, 1980]. In the following discussion we will assume that the hard X-ray source is isotropic and that the contributions of effects such as photospheric back-scattering to the observed X-ray spectra are negligibly small. The results obtained in this paper are not critically dependent on this assumption.

Interpretation of the hard X-ray emission in terms of thick-target bremsstrahlung from nonrelativistic electrons has been discussed in the literature [*Arnoldy et al.*, 1968; *Brown*, 1971; *Hudson et al.*, 1978]. If dN_e/dE_e were the rate (electrons $\sec^{-1}$ keV^{-1}) at which electrons are injected isotropically in a thick-target source, the photon flux at the earth is given by

$$\frac{dj}{dE} \approx 3.87 \times 10^{-34} \frac{1}{E} \int_{E}^{E_{emax}} dE_e \int_{E}^{E_e} dE_e' \frac{dN_e}{dE_e} \cdot \ln\left[\left(\frac{E_e'}{E}\right)^{1/2} + \left(\frac{E_e'}{E} - 1\right)^{1/2}\right] \quad (4)$$

photons cm^{-2} sec^{-1} keV^{-1}

where we have used the Bethe-Heitler formula for the bremsstrahlung cross-section. If the electron spectrum is a power law, the photon spectrum is also found to be a power law.

The relationship between a power law X-ray spectrum of the form

$$\frac{dj}{dE} = KE^{-\gamma} \quad \text{photons cm}^{-2}\,\text{sec}^{-1}\,\text{keV}^{-1} \quad (5)$$

observed at 1 AU and the corresponding power law electron spectrum

$$\frac{dN_e}{dE_e} = AE_e^{-\delta} \quad \text{electrons sec}^{-1}\,\text{keV}^{-1} \quad (6)$$

injected into the X-ray source is given by *Brown* [1971] and by *Hudson, Canfield and Kane* [1978]:

$$\delta = \gamma + 1 \quad (7)$$

$$A = 3.28 \times 10^{33}\, Kb(\gamma) \quad (8)$$

where

$$b(\gamma) = \gamma^2(\gamma - 1)^2 B\left(\gamma - \frac{1}{2}, \frac{3}{2}\right) \quad (9)$$

Here $B(x, y)$ is the Beta function.

In the case of a double power law X-ray spectrum of the form given in equation (1), the above relationships can be used directly for X-ray and electron energies above the break-point energy E_B. Even if there are no electrons with energy $E_e < E_B$, the above electron spectrum will produce X-rays with energy $\leq E_B$, although the magnitude of the X-ray flux will, in most cases, be much smaller than the flux actually observed. Electrons below E_B are therefore necessary to provide the additional X-ray flux below E_B actually observed. Numerical integration of equation (4) indicated that, to a first approximation, the complete electron spectrum corresponding to a double power law X-ray spectrum is also consistent with a double power law with the relationships similar to those given by equations (5) through (9). The break-point energy E_{eB} for the electron spectrum was, however, found to be larger than that (E_B) for the

X-ray spectrum.

The electron spectrum responsible for the X-ray spectrum given by equation (1) was assumed to have the form

$$\frac{dN_e}{dE_e} = \begin{cases} A_1 E_e^{-\delta_1} & \text{for } E_e \leq E_{eB} \\ A_2 E_e^{-\delta_2} & \text{for } E_e \geq E_{eB} \end{cases} \qquad (10)$$

electrons $\text{sec}^{-1}\ \text{keV}^{-1}$

The parameters δ_1, δ_2, A_1, A_2, and E_{eB} were computed using the following relationships:*

$$\delta_1 = \gamma_1 + 1 \qquad (11)$$

$$\delta_2 = \gamma_2 + 1 \qquad (12)$$

$$A_2 = 3.28 \times 10^{33}\ K_2\ b(\gamma_2) \qquad (13)$$

$$E_{eB} \approx E_B + 20 \qquad (14)$$

$$A_1 = A_2\ E_{eB}^{-(\gamma_2 - \gamma_1)} \qquad (15)$$

Table 2 presents the rate of injection N_e of electrons with energy $\gtrsim$25 and 100 keV into the X-ray source, deduced from the X-ray spectra observed at the seven peaks and valleys. As expected, N_e is larger at the peaks than at the valleys, the magnitude of the variation being much larger for electrons $\gtrsim$100 keV than for those $\gtrsim$25 keV.

V. ELECTRON–X-RAY–MICROWAVE RELATIONSHIP

The spatially resolved measurements of other flares indicate that the hard X-ray emission originates mostly in a thick-target source located low in the solar atmosphere where the ambient density is $\gtrsim 10^{12}\ \text{cm}^{-3}$. Any microwave emission which might originate in such a region is not expected to be detectable at 1 AU because of large absorption close to the source. Most models of the microwave source assume the ambient density to be $\lesssim 10^{10}\ \text{cm}^{-3}$ [*Takakura and Kai*, 1966; *Takakura*, 1972; *Ramaty*, 1973; *Matzler et al.*, 1978]. The physical locations of the hard X-ray and microwave sources are therefore expected to be different, with the microwave source at a higher altitude (lower ambient density) than the hard X-ray source. The population of

*A more general procedure, where δ_1 and E_{eB} are free parameters, has also been developed and will be reported elsewhere.

energetic electrons which produces the microwave emission is thus different from that which produces hard X-rays. The well-known close relationship between the hard X-ray and microwave emissions [*Kundu*, 1961; *Arnoldy et al.*, 1968; *Kane*, 1973] would then require a common acceleration process for the two electron populations. Hence, the rate of electron injection deduced from the observed hard X-ray spectra can be considered a measure of the rate of electron injection into the microwave source.

In order to examine the relationship between the hard X-rays, microwave emission and energetic electrons in some detail, the X-ray data during the period 0312:04-0313:03 UT were averaged over one second. At the times $t_1, t_2, \ldots, t_{60}$ corresponding to these data averages, double power law X-ray spectra were fitted to the observations and the rates of injection of electrons $\gtrsim$ 25 keV and $\gtrsim$ 100 keV were computed as described in the last section. Also the 17 GHz flux values at these times were obtained from the radio observations. These data formed the basis for the following analysis.

(a) General correlations

The first part of the analysis consisted of the computation of the cross-correlation coefficients among several variables: 26 - 121 keV and 121 - 398 keV X-ray counting rates, 17 GHz radio flux, and the injection rates of electrons $\gtrsim$ 25 keV and $\gtrsim$ 100 keV. Either the variables were used in their normal form (linear-linear correlation) or the logarithm of the variables to the base 10 was obtained before the correlation coefficients was computed (log-log correlation). Because of the large magnitude of the variations in the X-ray counting rates compared to those in the microwave emission, only the logarithms of the X-ray rates were used for the correlation analysis. A total of 60 pairs of values was used in each case. The correlation coefficient matrix is shown in Table 3. The probabilities of obtaining correlation coefficients larger than 0.3 and 0.45 by chance alone are 0.02 and 0.001, respectively [*Bevington*, 1969]. In general the log-log or log-linear correlation coefficient is larger than the linear-linear correlation coefficient, although good correlation, where it exists, can be clearly inferred in either case. The correlation of the 17 GHz flux with the rates of 26 - 121 keV X-rays, 121 - 398 keV X-

Table 3. Correlation Coefficients (7 June 1980)

Quantity	X-ray Rate 26-121 keV		X-ray Rate 121-398 keV		Electron Rate ≥ 25 keV		Electron Rate ≥ 100 keV	
	Log	Lin	Log	Lin	Log	Lin	Log	Lin
17 GHz Radio Flux								
Log	0.91		0.93		0.46		0.81	
Lin	0.88	0.84	0.95	0.88	0.38	0.30	0.84	0.69
X-ray Rate								
26-121 keV								
Log			0.97		0.64		0.89	
Lin						0.56		0.89
121-398 keV								
Log					0.47		0.93	
Lin						0.44		0.85

Note: The probabilities of obtaining correlation coefficients larger than 0.3 and 0.45 by chance are 2% and 0.1%, respectively.

rays, and $\gtrsim$ 100 keV electrons is very good, as indicated by the corresponding log-log correlation coefficients 0.91, 0.93, and 0.81, respectively. The log-log correlation coefficient between the 17 GHz flux and $\gtrsim$ 25 keV electron rate is substantially smaller (0.46).

(b) Time delay

A preliminary examination of the X-ray and microwave data indicated a possible time delay between the characteristic features of the time-intensity profiles, such as peaks and valleys. Since the width of these features is up to several seconds, however, an unambiguous conclusion could not be drawn from the primary data. In order to clarify the situation, the correlation coefficients $r(\tau)$ of the X-ray and electron rates with the 17 GHz radio flux were computed as a function of the time delay τ(sec), artificially introduced between the X-ray or electron rates and the radio flux. A total of 21 values of τ, varying from -10 to $+10$ sec, was used. In each case, the log-log correlation coefficient was computed from forty pairs of data.

Figure 8(a) shows the results for 26 - 121 keV and 121 - 398 keV X-rays. The dependence of the correlation coefficient $r(\tau)$ on τ is asymmetrical with respect to $\tau = 0$. As τ increases from -10 sec to $+10$ sec, $r(\tau)$ increases rapidly, reaches a maximum at $\tau = 0$ or 1 sec and then decreases slowly. Since there is no obvious time difference in the onset of the two emissions, this asymmetric behaviour of $r(\tau)$ is probably caused by the differences in the rise and decay times of the radio flux as compared to those for the X-ray rates. There is an indication that the radio emission is delayed by $\sim$ 1 sec with respect to the X-rays. Figure 8(b) shows similar results for the injection rates of electrons $\gtrsim$ 25 keV and $\gtrsim$ 100 keV deduced from the X-ray observations. Again, the radio emission lags behind the electron injection rate by $\sim$ 1 sec.

The observed delay is comparable to the 1 sec averaging time for the X-ray data but is larger than the uncertainty ($\lesssim$ 0.5 sec) in the absolute timing of the X-ray and radio data. Hence the present observations are consistent with the 17 GHz emission at the sun being delayed by $\sim$ 1 sec. with respect to the hard X-ray emission or the injection rate of energetic electrons.

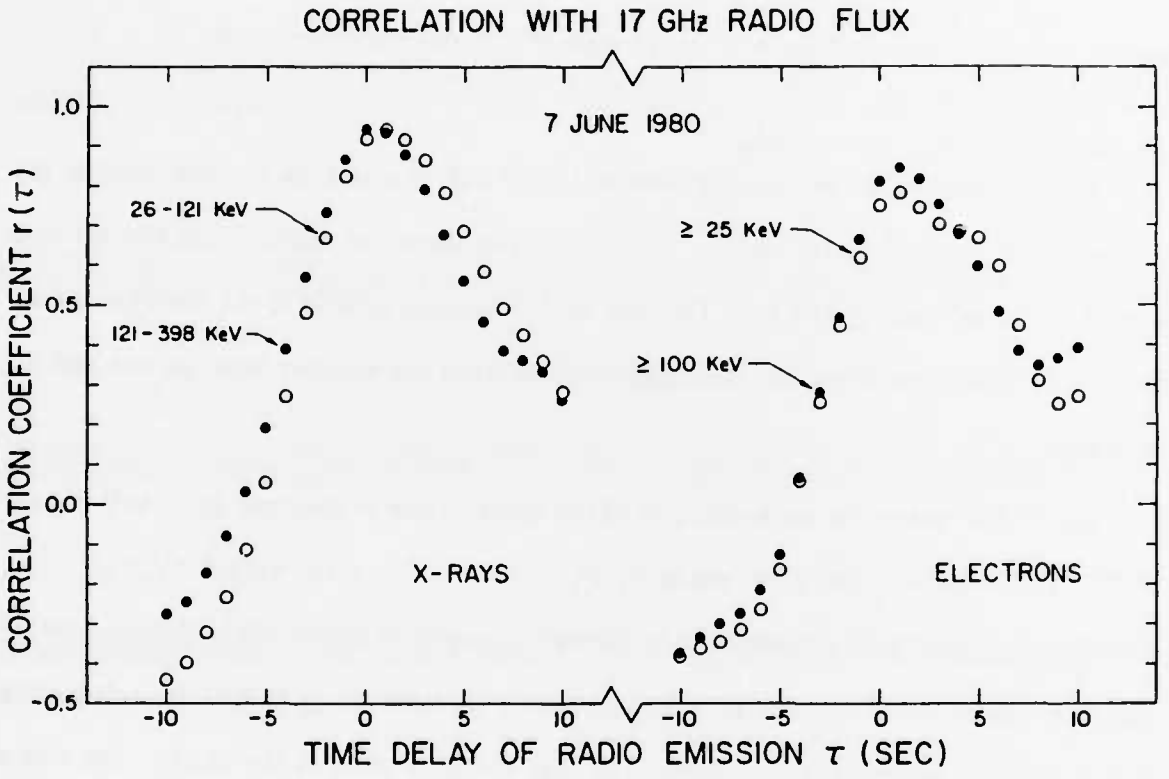

Figure 8. Correlation of 17 GHz radio flux with hard X-rays and energetic electrons as a function of the delay introduced between the different data sets. Note (1) the correlation is maximum for the delay $\simeq$ 1 sec. (2) the dependence of the correlation coefficient on the delay is asymmetric with respect to delay = 0.

The above interpretation of the apparent time delay between the X-ray and microwave emissions is not unique. For example, an X-ray peak at a time t_0 may correspond to two microwave peaks, one at time t_0 and the other at time $t_0 + \Delta t$ where $\Delta t \simeq 2$ sec. A cross-correlation analysis will show the presence or absence of a delay, depending on the relative magnitudes of the two microwave peaks. Since the microwave peaks in the 7 June 1980 flare are several seconds wide, it is not possible to rule out such a possibility. In the following discussion we assume that an X-ray peak corresponds to only one microwave peak.

(c) Electron−Microwave Relationship

We now consider the relationship between the 17 GHz flux and the electron injection rate deduced from the hard X-ray spectra. As before, two ranges of electron energies are considered, $\gtrsim$ 25 keV and $\gtrsim$ 100 keV. The data used correspond directly to the observed quantities. No artificial time delay has been introduced between the electron injection rate and the radio flux.

Figure 9(a) shows the regression plot of the injection rate of electrons $\gtrsim$ 25 keV and the 17 GHz flux at times of the seven peaks $P_1, P_2, \cdots P_7$ and the seven valleys $V_1, V_2, \cdots V_7$. A similar regression plot for electrons $\gtrsim$ 100 keV is shown in Figure 9(b). Whereas the 17 GHz flux appears to have little or no relationship with the electrons $\gtrsim$ 25 keV, the relationship with $\gtrsim$ 100 keV electrons is very good. The data points lie close to the straight line, which represents a relationship where the radio flux is proportional to the square-root of the injection rate of electrons $\gtrsim$ 100 keV.

In order to examine this relationship in some detail, we present in Figure 10 the regression plot of the $\gtrsim$ 100 keV electron rate and 17 GHz flux for all 64 data pairs, covering the entire event (0312:04-0313:07 UT). The data points before and after the first peak P_1 have been denoted by open and closed (full) circles, respectively. It can be seen that, for a given electron injection rate, the radio flux is much *smaller* during the *initial rise* to the first peak P_1 than after P_1. The relationship after P_1 is consistent with the straight line

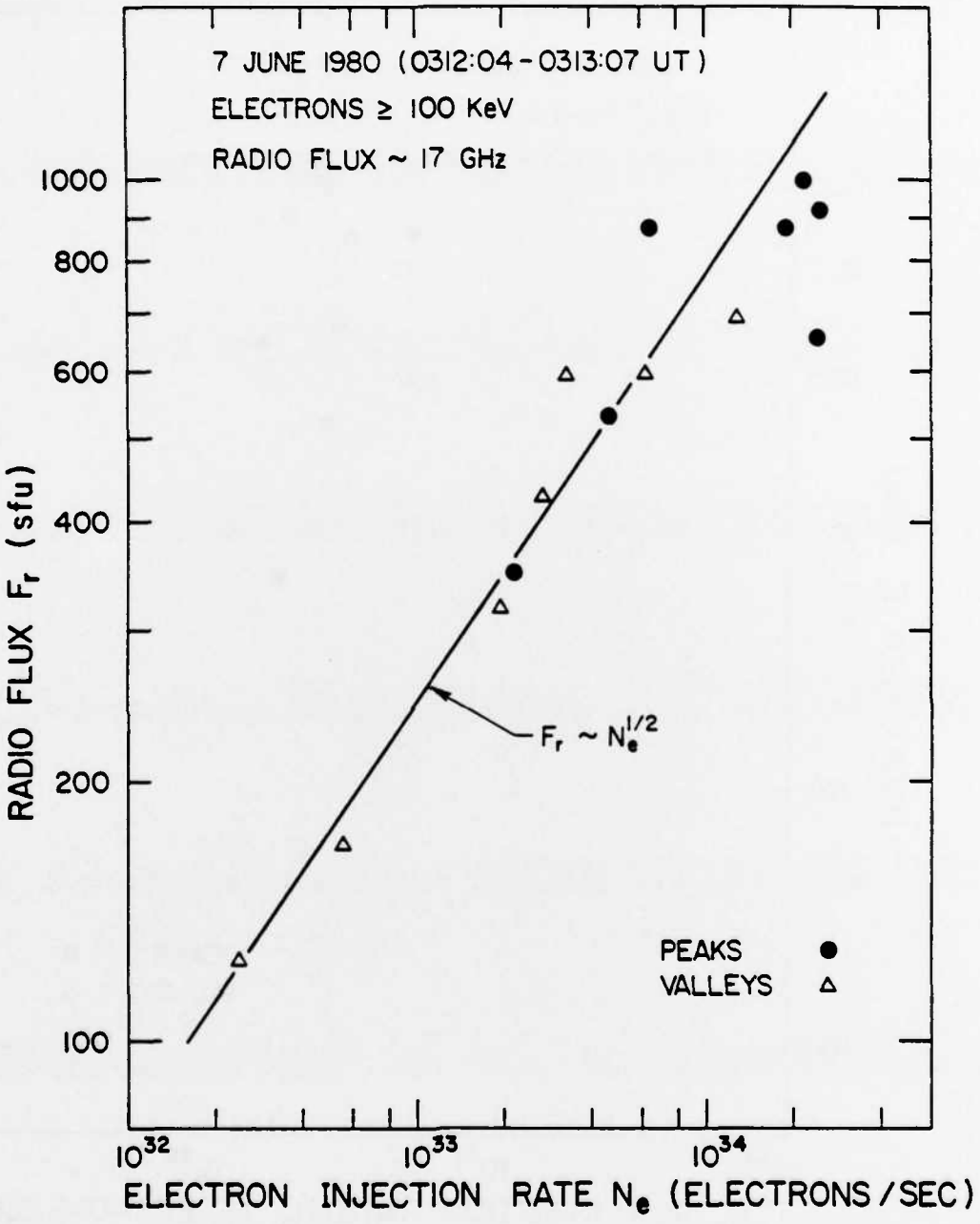

Figure 9. (a) Regression plot of the 17 GHz radio flux against the injection rate of electrons $\gtrsim$ 25 keV at times of the seven peaks and valleys.

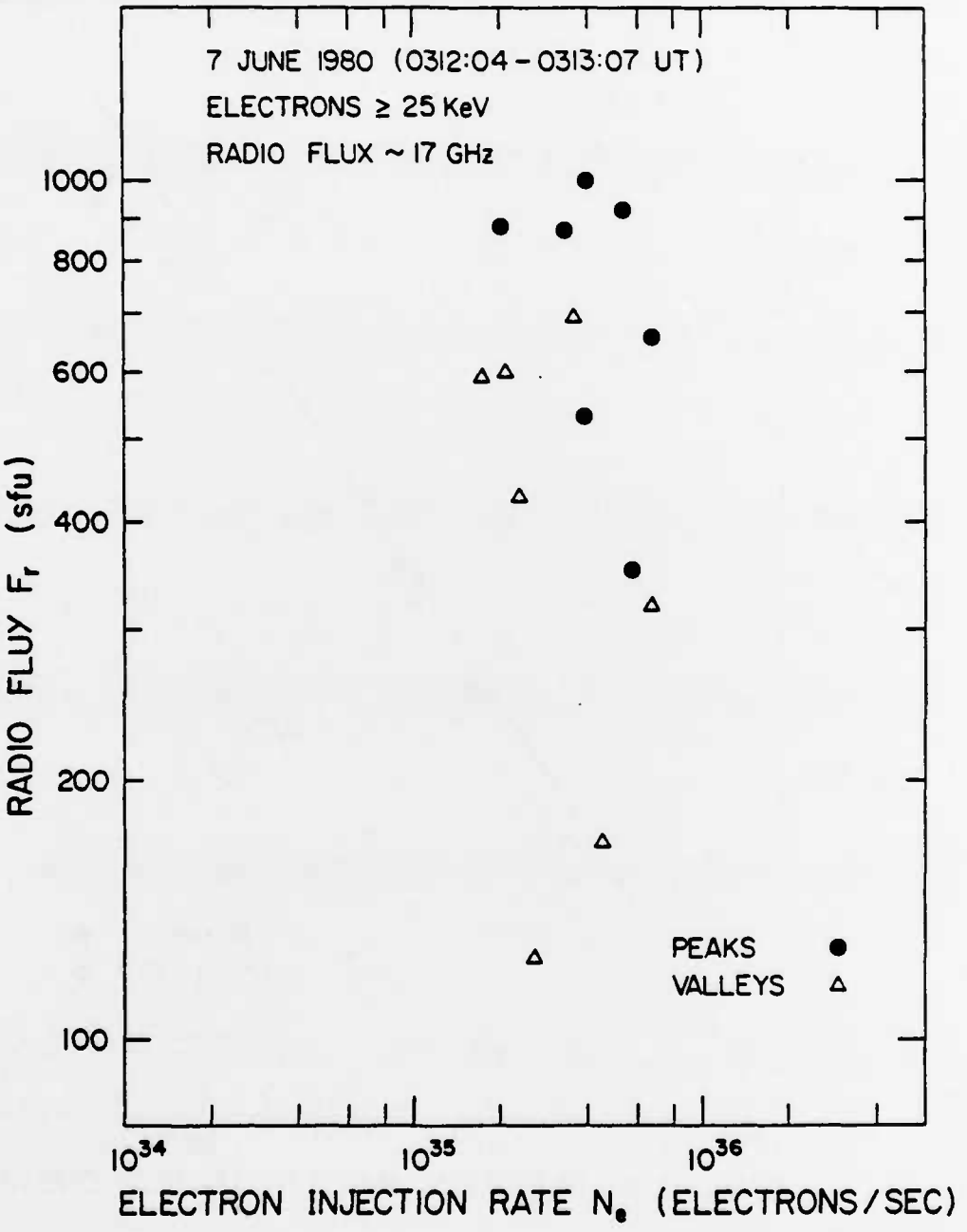

Figure 9. (b) Same as (a) but electrons > 100 KeV. Note that the radio flux is much better correlated with electrons > 100 keV than with electrons > 25 keV.

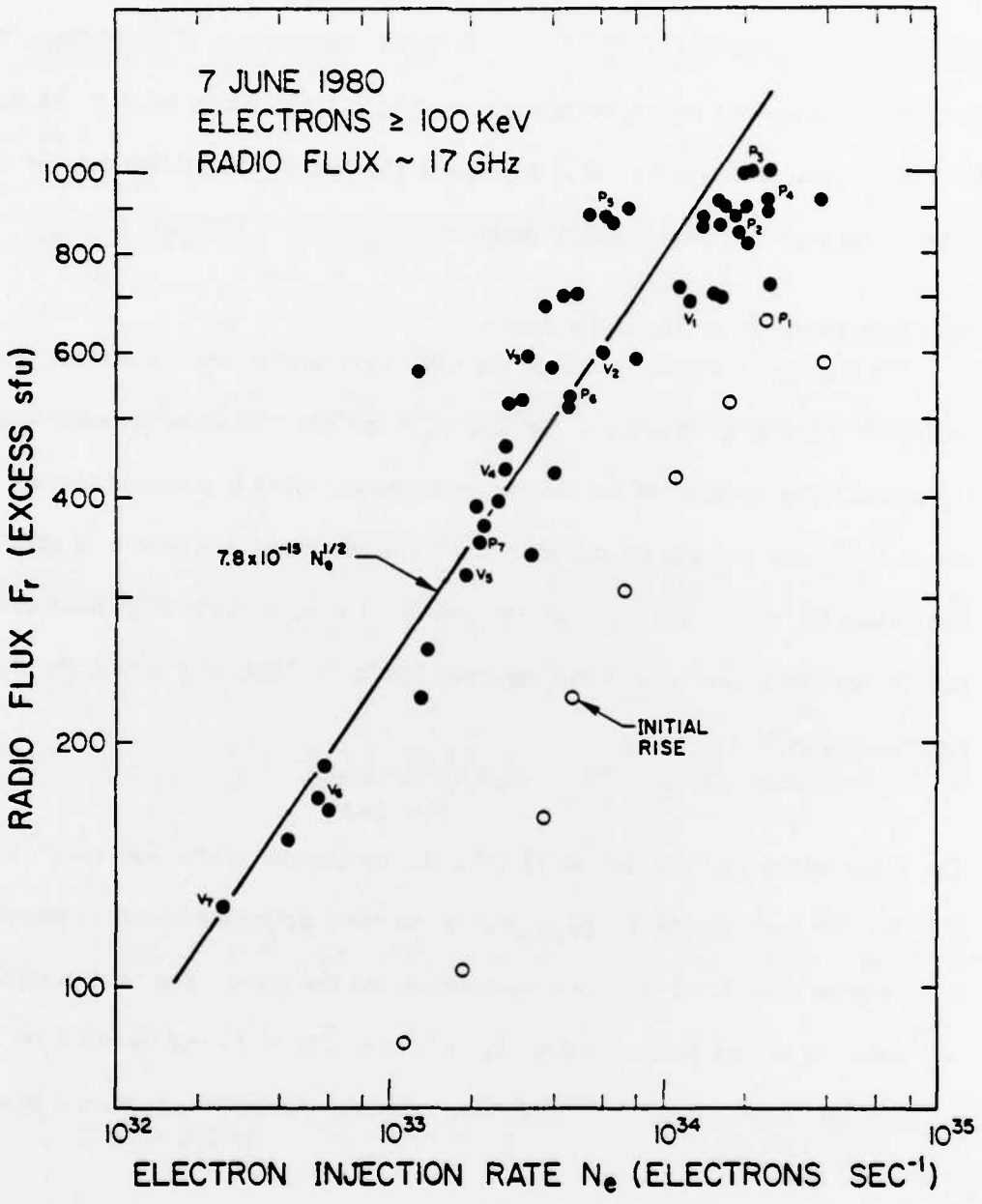

Figure 10. Regression plot of the 17 GHz radio flux against the injection rate of electrons ≥ 100 keV. All data points during the event, including the peaks and valleys, have been plotted. The straight line is the same as in Figure 9(b). Note (1) the relationship is different before the first peak P_1 (open circles) from that after P_1 (full circles). (2) After P_1 the radio flux varies approximately as the square root of the electron injection rate.

$$F_r \approx 7.8 \times 10^{-15} N_e^{1/4} \tag{16}$$

where F_r is the radio flux at 17 GHz and N_e is the injection rate of electrons $\gtrsim$ 100 keV. It is important to note that the above relationship does not necessarily apply to the times between individual peaks and valleys. (16) represents the overall relationship for the time interval between the peak P_1 and the end of the event.

(d) Characteristics of the Microwave Source

We consider a simple model of the microwave source where electrons $\gtrsim$ 100 keV are injected at a rate βN_e. β is a constant and N_e is the rate of electron injection into the hard X-ray source. The intensity of the microwave emission, which is produced through the gyrosynchrotron process, depends on the total number of electrons, magnetic field structure, ambient plasma density, etc., inside the source volume V. Let n_e be the average number density and τ the average life time of $\gtrsim$ 100 keV electrons inside V. Then, at a time t, the total number of electrons inside V is given by

$$n_e V \approx \beta \tau N_e \tag{17}$$

The observations indicate that at 17 GHz the microwave source was stable, with a volume $V \lesssim 4 \times 10^{25}$ cm^3. Hence V and τ, both presumably determined by the magnetic field structure, may be considered essentially constant during the event. The total number of electrons $n_e V$ inside V is thus proportional to N_e. However, Figure 10 and equation (8) show that the 17 GHz flux varied as $\sim N_e^{1/4}$. This indicates that the microwave source was probably optically thick at 17 GHz.

The microwave spectra shown in Figure 7 are also consistent with the large optical thickness of the microwave source. Since $N_e \sim 10^{34}$ electrons cm^{-3} and $V \lesssim 4 \times 10^{25}$ cm^3, we find the average density of electrons $\gtrsim$ 100 keV to be

$$n_e \gtrsim 2.5 \times 10^8 \beta \tau \text{ electrons cm}^{-3} \tag{18}$$

Both β and τ are unknown. The rise and decay times of the microwave flux indicate that $\tau \sim 1$ sec. If we assume that at least 10% of the accelerated electrons are injected into the microwave source so that $\beta \tau \gtrsim 0.1$, we get $n_e \gtrsim 10^7$ cm^{-3}. This large density of energetic

electrons is expected to produce substantial gyrosynchrotron self absorption in the microwave source. An enhancement of the electron injection rate N_e will therefore enhance the gyrosynchrotron self absorption as well as the emission. The resultant net emission will therefore be less intense and the spectrum will peak at a frequency f_{max} much higher than that in the case of an optically thin source. At the valleys and during the overall decay of the flux, the electron injection rate is smaller. Consequently, the self absorption is reduced and hence f_{max} is expected to move to lower frequencies (cf. *Takakura,* 1972) as is indeed observed. A decrease in the optical thickness will increase the relative contribution of the extraordinary mode to the net emission. This is consistent with the observed increase in the circular polarization at the valleys and also with the overall increase in the polarization with the gradual decrease in the 17 GHz flux during the event.

(e) Hard X-Ray and Microwave Source Structure

As far as the detailed structure of the hard X-ray and microwave sources is concerned, a number of possibilities exist, including a common source for the X-ray and microwave emissions and more than one sub-source (kernel) in the X-ray and microwave source regions. We have already mentioned that the spatially resolved hard X-ray observations of other flares indicate that the X-ray source is located low in the solar atmosphere where the ambient density is high ($\gtrsim 10^{12}\,cm^{-3}$). Hence the microwave source, which requires much lower ambient density for the radiation to escape, is expected to be physically separate from the principal part of the hard X-ray source.

Spatially resolved hard X-ray measurements are not available for the 7 June 1980 flare. It is therefore not possible to determine if the hard X-ray emission originated from one or more sources. The measurements at 17 GHz, however, did have good spatial resolution and hence we can obtain upper limits on the microwave source size. For the discussion in the last section, we assumed that a single microwave source was responsible for the entire radio flux profile. This simple assumption is consistent with the 17 GHz observations, which indicate a compact and stable source region <5" in size. It is possible, however, that more than one "point"

source (kernel), each of size ~1", existed in the source region. For example, the emission at the peaks and valleys could have been produced by two different sources, one source producing the rapidly fluctuating component and the other producing the slowly decaying gradual component. As an extreme case, one might invoke the existence of seven separate and independent point sources to explain the seven emission peaks. This could result from a successive "triggering" of very small magnetic loops (~ few arc sec) in an arcade. The present observations are unable to confirm or reject such models involving point sources. The analysis presented here does show, however, that a single compact microwave source is consistent with the observations.

A variety of models have been proposed to explain the hard X-ray microwave relationship (cf. *Kane*, 1980). If both the hard X-ray and microwave emissions are produced by precipitating electrons (cf. Fig. 3 of *Kai*, 1982), it is possible to have a low altitude X-ray source and compact microwave source, but no delay is expected between the two types of emissions. On the other hand, if both emissions are produced by trapped electrons [*Ramaty*, 1973; *Takakura*, 1972; *Matzler et al.*, 1978], the X-ray source will be located at a relatively high altitude (low density) above the photosphere. Magnetic traps have been invoked in the past to obtain temporal variations in the injected electron spectrum through escape, energy loss and/or acceleration [*Brown and Hoyng*, 1975; *Vilmer, Kane, and Trottet*, 1982]. It appears that a partial precipitation model [*Kane*, 1974; *Melrose and Brown*, 1976] could explain the observations if the trapping geometry provided an effective delay of ~ 1 sec in the build-up of the electron pitch angle distribution and energy spectrum most efficient for microwave emission.

VI. PARTICLE ACCELERATION PROCESS

Acceleration of particles in solar flares is often discussed in terms of two "phases". In the first phase, which coincides in time with the impulsive phase of a flare, particles are accelerated to relatively low energies. For example, 10 keV to several hundred keV electrons with a relatively steep spectrum are produced in the first phase. The higher energy electrons

with considerably harder spectrum and energetic protons and heavier nuclei are produced presumably several minutes later in the second phase (cf. *Ramaty et al.*, 1980). A second "step" acceleration, which follow the first "step" or "phase" by a few seconds, is sometimes invoked to explain the acceleration of protons and heavier nuclei during or close to the impulsive phase [*Bai*, 1982]. Below we examine briefly the 7 June 1980 flare observations to determine which "phases" or "steps" of acceleration might be applicable to the event.

Since the various phases or steps of acceleration are distinguished on the basis of timing and spectra of the accelerated particles, the relevant observational characteristics are as follows:

1. The total duration of the hard X-ray and microwave bursts is relatively short ($\sim$ 80 sec).

2. The first emission peak is a part of the fluctuations.

3. The spectrum of the gradual X-ray component (the envelope of the peaks or valleys) tends to soften with time.

4. The radio spectrum at the peaks is much steeper than that associated with the gradual (extended) hard X-ray bursts which follow the impulsive bursts in large flares [*Stewart and Nelson*, 1980].

5. Production of energetic ($\gtrsim$ 30 MeV) ions has been inferred from the observations of the gamma-ray line emission in the 4.1 - 6.4 MeV range, which has a time-intensity profile similar to that of the hard X-ray emission, but the gamma-ray peaks are delayed with respect to the corresponding X-ray peaks by $\sim$ 1 sec [*Forrest et al.*, 1981].

6. The onset of a type II (metric) radio burst is $\sim$ 1 min after the onset of the hard X-ray burst.

The overall appearance of the time-intensity profile, its short duration and the relatively steep radio spectrum indicate that the 7 June 1980 flare (Figure 1) represents the impulsive phase (first phase) acceleration. Although the production of a type II radio burst and energetic ions is usually associated with the second phase acceleration, the time delay of $\sim$ 1 sec between

the hard X-ray and gamma ray line emission peaks is too small compared with the delay of several minutes usually expected in the case of the second phase acceleration. The small delay of $\sim$ 1 sec has been considered by *Bai* [1981] as evidence for the second "step" acceleration for high energy electrons and ions. He has argued that in this event, the second step acceleration did not influence electrons with energies up to $\sim$ 400 keV and hence, high energy X-rays were not delayed with respect to low energy X-rays. On the basis of the present observations we are unable to confirm or rule out such a possibility. The observations, however, are consistent with a process where both electrons and ions are accelerated simultaneously during the impulsive phase. The differences in the rates of energy gain and loss could explain the small differences in the rise times and times of maxima for these particles.

VII. SUMMARY AND CONCLUSIONS

1. The event has a total of seven well defined peaks, with an average separation of $\sim$8 sec between the peaks.

2. In the X-ray emission $\gtrsim$20 keV there is no indication of a fine time structure with a time constant of $\gtrsim$ 0.032 sec.

3. There is a general similarity between the time intensity profiles of 26 - 398 keV X-rays and 9.4 - 17 GHz radio emission, the similarity decreasing substantially with the decrease in the X-ray energy below 26 keV and with the decrease in frequency below 9.4 GHz. There is some indication of the radio emission lagging behind the X-ray emission by $\sim$1 sec.

4. The logarithmic amplitude of the variations is much smaller for X-rays $\lesssim$ 43 keV than that for higher energy X-rays.

5. The spectrum of X-rays $\gtrsim$ 20 keV tends to harden with time during the initial increase of the X-ray emission, then hardens at the intensity peaks and softens at the intensity valleys.

6. The spectrum of the microwave radio emission is relatively steep at the intensity peaks and has a maximum at frequencies $f_{max} \gtrsim$ 17 GHz. At the valleys the spectrum is relatively less steep and $f_{max} \lesssim$ 17 GHz. For both peaks and valleys, f_{max} (and hence the steepness of

the spectrum) decreases systematically with time.

7. The polarization of 17 GHz emission is small (5-10%) at intensity peaks and relatively larger (10-20%) at intensity valleys.

8. The size of the radio source at 17 GHz is $\lesssim 5''$. Both the size and the position of the source did not change significantly during the event.

9. The injection rate N_e of $\gtrsim$ 100 keV electrons deduced from the hard X-ray spectra is well correlated with the 17 GHz flux F_r. After the first emission peak, the overall relationship between N_e and F_r is of the form and $F_r \sim N_e^{1/4}$.

10. The observations are consistent with a model in which X-rays originate at low altitudes in a thick-target bremsstrahlung source and the microwaves are produced through the gyrosynchrotron process in a source located at higher altitudes. At frequencies $\lesssim$ 17 GHz, the microwave source is optically thick, the thickness increasing with the increase in the electron injection rate. The electrons exciting the X-ray and the microwave emissions as well as the ions responsible for the gamma-ray line emission are energized in a common acceleration process during the impulsive phase of the flare. A modulation of the particle injection/acceleration rate probably produces the observed fluctuations in the microwave, X-ray and gamma-ray emissions.

References

Anderson, K. A., and Mahoney, W.A., 1974, *Solar Phys.* 35, 419.

Arnoldy, R. L., Kane, S. R., and Winckler, J. R., 1968, *Ap. J.* **151**, 711.

Bai, T., 1982, in *Gamma-Ray Transients and Related Astrophysical Phenomena*, edited by R. E. Lingenfelter, H. S. Hudson, and D. M. Worrall (New York: American Institute of Physics) p. 409.

Bevington, P.R., 1969, *Data Reduction and Error Analysis for the Physical Sciences* (New York: McGraw-Hill), Chapter 7.

Brown, J. C., 1971, *Solar Phys.* **18**, 489.

Brown, J. C., and Hoyng, P., 1975, *Ap. J.* **200**, 734.

Chupp, E. L., Forrest, D. J., Ryan, J. M., Cherry, M. L., Reppin, C., Kanbac, G., Rieger, E., Pinkau, K., Share, G. H., Kinzer, R. L., Strickman, M. S., Johnson, W. H., and Kurfess, J. D., 1981, *Ap. J. Letters* **244**, L171.

Frost, K. J., 1969, *Ap. J. Letters* **158**, 1159.

Frost, K. J., and Dennis, B. R., 1971, *Ap. J.* **165**, 655.

Hoyng, P., Duijveman, A., Machado, M. E., Rust, D., M., Svestka, Z., Boelee, A., de Jager, C., Frost, K. J., Lafleur, H., Simnett, G. M., van Beek, H. F., and Woodgate, B. E., 1981, *Ap. J.* **246**, L155.

Hudson, H. S., Canfield, R. C., and Kane, S. R., 1978, *Solar Phys.* **60**, 137.

Hurley, K., and Duprat, G., 1977, *Solar Phys.* **52**, 107.

Kai, K., 1982, *Proc. HINOTORI Symp. on Solar Flares* Tokyo.

Kane, S. R., 1973, in *High Energy Phenomena on the Sun*, edited by R. Ramaty and R. G. Stone, NASA SP-342, p. 55.

Kane, S. R., 1980, *Ap. Space Sci.* **75**, 163.

Kane, S. R., and Anderson, K. A., 1970, *Ap. J.* **162**, 1003.

Kane, S. R., Anderson, K. A., Evans, W. D., Klebesadel, R. W., and Laros, J. G., 1980, *Ap. J. Lett.* **239**, L85.

Kane, S. R., Landecker, P. B., and McKenzie, D. L., 1982, Aerospace Corp. Space Sci. Lab. Report No. SSL-82(2940-01)-5.

Kane, S. R., Crannell, C. J., Datlowe, D. W., Feldman, U., Gabriel, A., Hudson, H. S., Kundu, M. R., Mätzler, C., Neidig, D., Petrosian, V., and Sheely, Jr., N. R., 1980, *Solar Flares*, edited by P. Sturrock (Boulder: Colorado Associated University Press) p. 187.

Kane, S. R., Kai, K., and Enome, S., 1980, *Bull. A. A. S.* **12**, 889.

Kane, S. R., Fenimore, E. E., Klebesadel, R. W., and Laros, J. G., 1982, *Ap. J. Letters* **254**, L53.

Kiplinger, A. L., Dennis, B. R., Frost, K. J., and Orwig, L. E., 1980, *Bull. A. A. S.* 12, 889.

Kosugi, T., 1982, Public Astron. Soc. Japan, (in press).

Kundu, M. R., 1961, *J. Geophys. Res.* 66, 4308.

Kundu, M. R., 1965, *Solar Radio Astronomy,* (New York: Intersci. Publ.), p. 42.

Landecker, P. B., McKenzie, D. L., and Rugge, H. R., 1979, *Proc. SPIE* 184, 285.

Lipa, B., 1978, *Solar Phys.* 57, 191.

Matzler, C., Bai, T., Crannell, C. J., and Frost, K. J., 1978, *Ap. J.* 223, 1058.

Melrose, D. B., and Brown, J. C., , 1976, *Mon. Nat. Roy. Astron. Soc.* 176, 15.

Nakajima, H., Sekiguchi, H., Aiba, S., Shiomi, Y., Kuwabara, T., Sawa, M., Hirabayashi, H., Kosugi, T., and Kai, K., 1980, *Pub. Astr. Soc. Japan* 32, 639.

Parks, G. K., and Winckler, J. R., 1969, *Ap. J. Letters* 155, L117.

Ramaty, R., 1973, in *High Energy Phenomena on the Sun,* edited by R. Ramaty and R. G. Stone, NASA SP-342, p. 188.

Stewart, R. T., and Nelson, G. J., 1980, *Proc. Astron. Soc. Australia* 3, 380.

Takakura, T., 1972, *Solar Phys.* 26, 151.

Takakura, T., and Kai, K., 1966, *Pub. Astr. Soc. Japan* 18, 57.

Torri, C., Tsukiji, Y., Kobayashi, S., Yoshimi, N., Tanaka, H., and Enome, S., 1979, *Proc. Res. Inst. Atmospherics, Nagoya Univ.* 26, 129.

Vilmer, N., Kane, S. R., and Trottet, G., 1982, *Astron. Astrophys.* 108, 306.

LABORATORY OPERATIONS

The Laboratory Operations of The Aerospace Corporation is conducting experimental and theoretical investigations necesaary for the evaluation and application of scientific advances to new military space systems. Versatility and flexibility have been developed to s high degree by the laboratory personnel in dealing with the many problems encountered in the nation's rapidly developing space systems. Expertise in the latest scientific developments is vital to the accomplishment of tasks related to these problems. The laboratories that contribute to this research are:

Aerophysics Laboratory: Launch vehicle and reentry aerodynamics and heat transfer, propulsion chemistry and fluid mechanics, structural mechanics, flight dynamics; high-temperature thermomechanics, gss kinetics and radistion; research in environmental chemistry and contamination; cw snd pulsed chemical laser development including chemical kinetics, spectroscopy, optical resonators and beam pointing, atmospheric propagation, laser effects and countermeasures.

Chemistry and Physics Laboratory: Atmospheric chemical reactions, atmospheric optics, light scattering, state-specific chemical resctions and radiation transport in rocket plumes, applied laser spectroacopy, laser chemistry, battery electrochemiatry, space vacuum and rsdiation effects on materials, lubrication and surface phenomens, thermionic emission, photosensitive materials and detectors, atomic frequency standards, and bioenvironmental research and monitoring.

Electronics Research Laboratory: Microelectronics, GaAs low-noise and power devices, semiconductor lasers, electromagnetic and optical propagation phenomena, quantum electronics, laser communications, lidar, and electro-optics; communication sciencea, applied electronics, semiconductor crystal and device physics, radiometric imaging; millimeter-wave and microwave technology.

Information Sciences Research Office: Program verification, program translation, performance-sensitive system design, distributed architectures for spaceborne computers, fault-tolerant computer systems, artificial intelligence, snd microelectronics applications.

Materials Sciences Laboratory: Development of new materials: metal matrix composites, polymers, and new forms of carbon; component failure analysis and reliability; fracture mechanics and stress corrosion; evaluation of materials in space environment; materials performance in space transportation systems; analysis of systems vulnerability and survivability in enemy-induced environments.

Space Sciences Laboratory: Atmospheric and ionospheric physics, radiation from the atmosphere, density and composition of the upper atmosphere, aurorae and airglow; magnetospheric physics, cosmic rays, generation and propagation of plasma waves in the magnetosphere; solar physics, infrared astronomy; the effects of nuclear explosions, magnetic storms, and solar activity on the earth's atmosphere, ionosphere, and magnetosphere; the effects of optical, electromagnetic, and particulate radistions in space on space systems.

• • •

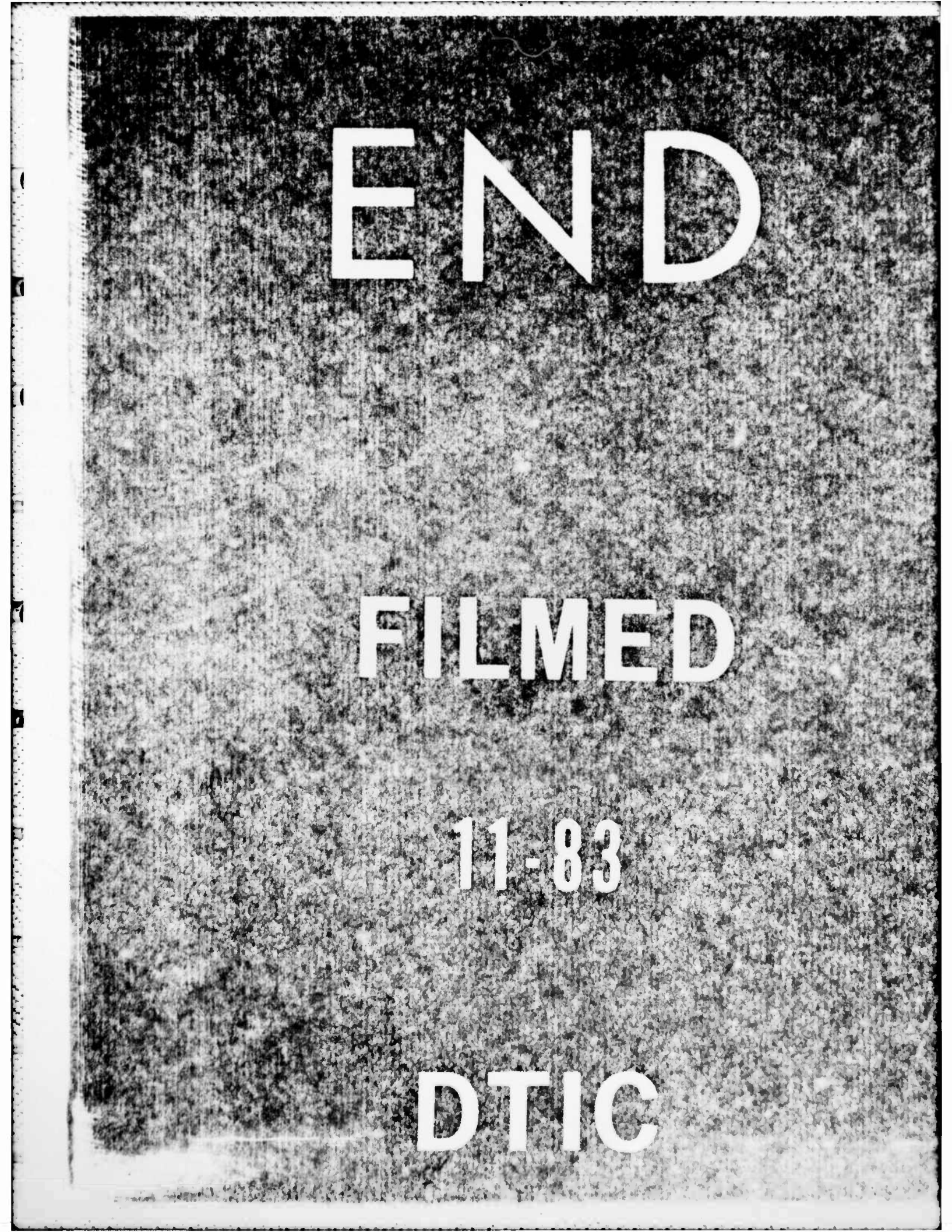
END
FILMED
11-83
DTIC